PROCEEDINGS
SPIE—The International Society for Optical Engineering

Practical Holography VI

Stephen A. Benton
Chair/Editor

11–13 February 1992
San Jose, California

Sponsored by
SPIE—The International Society for Optical Engineering
IS&T—The Society for Imaging Science and Technology

Published by
SPIE—The International Society for Optical Engineering

Volume 1667

Automatic particle sizing from rocket motor holograms

J.P. Powers* and David W. Netzer**

*Department of Electrical and Computer Engineering
**Department of Aeronautics and Astronautics
Naval Postgraduate School, Monterey, California 93943

ABSTRACT

Solid-propellant rocket fuels frequently have spherical aluminum pellets added to improve combustion efficiency and to improve thrust performance. In order to model the combustion process, information is required about the size of the particles as they lift off of the propellant surface. We have used optical pulsed-laser holography to record an approximate 2.5 cm x 2.5 cm x 2.5 cm volume at the propellant surface in a test rocket motor. A pulsed ruby laser, combined with a laser line filter to remove the flame light, records the hologram. A diffuser is used to remove the phase gradients introduced by the thermal effects in the flame. The scene is reconstructed a krypton laser, viewed with an optical microscope, and captured on videotape. The recorded scene is digitized and analyzed with digital image processing techniques on a personal computer equipped with an video memory board and an image processing subroutine library. The image processing techniques developed reduce the speckle in the scene, apply a threshold to differentiate the particles from the background, and locate and size the particles. Statistical analysis of the sizing results provides a histogram representation of the particle size distribution. Particle resolution down to 10 micrometers has been achieved with this technique.

1. INTRODUCTION

Investigations have been made to study the effects of addition of aluminum and other metallic particles on the magnitude of the performance losses in propellant motors[1,2,3]. The goal was to investigate the behavior of solid particulates (Al, Al_2O_3) (ranging in size from 0.1 to 100 μm) near to the burning fuel surface and within the exhaust nozzle. Motor performance and signature are sensitive to the particle size distribution throughout the rocket motor and nozzle. Data are required 1) to improve the solid-propellant performance, 2) to provide input to the current steady-state combustion models to describe the interactions between the ammonium perchlorate (AP) and the aluminum, and 3) to provide in-motor particle size distributions to allow more accurate predictions relating to exhaust plume formation. Since no size distribution data exists in these regions of the motor for evaluation of existing analytical models, direct observation has been undertaken to provide the needed information.

Single-pulse holography provides a means for effectively stopping the motion. However, it provides information only during an instant of time; information about preceding and successive instants of time are not available. Holography offers the advantage of eliminating the effects of flame light (through the use of laser-line filters) and thermal gradients (through the use of diffuse illumination) while recording a significant volume of the region under investigation. However, smoke generation during the combustion process presents a major obstacle to obtaining good holograms. Transmissions of 10% or more are required to successfully record a hologram and the desired ratio between the reference beam and the scene beam is difficult to maintain constant from test to test due the presence of a variable amount of smoke. To achieve an optimum combination of low levels of smoke within the combustion chamber with well-developed burning required experimental determination of the most suitable fuel sample dimensions and the optimum time to take the hologram after burn initiation.

Holographic techniques have been employed to capture the dynamics of the combustion chambers of small rocket motors while firing at pressures of 34 and 68 atm with various concentrations of aluminum up to 15%. Concurrently, improvements in the processing of the holograms to extract the particle size distributions were also necessary. Once the hologram has been successfully recorded, it was desirable to have a computer process the image to measure the particle size and to produce a statistical description of the particle size distribution[4].

0-8194-0821-2/92/$4.00

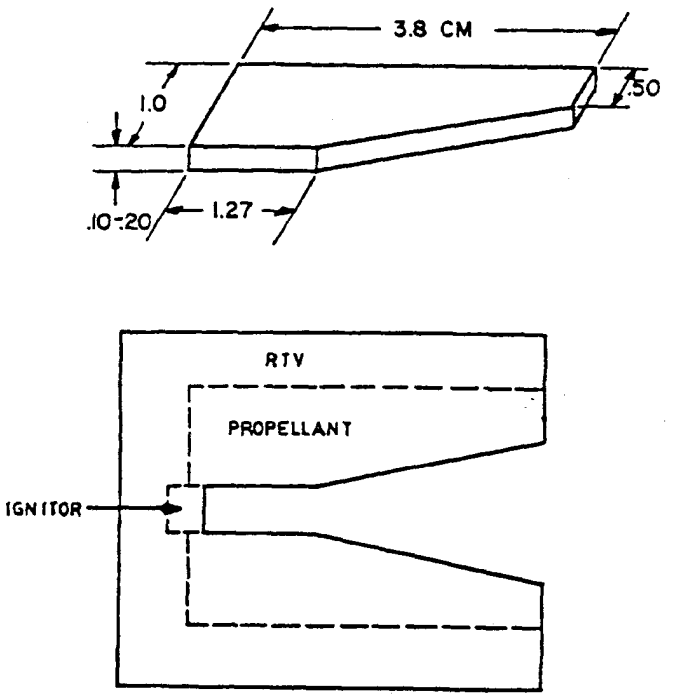

Figure 1: Two–dimensional fuel geometry.

2. MOTOR CONFIGURATIONS

Both a two–dimensional motor and a three–dimensional motor were used in the investigations. A nitrogen purge system directed nitrogen across the windows throughout the firing and hologram recording process. The laser was fired electronically by an electronic circuit with a variable time delay after the fuel ignition was initiated. A photodiode in the laser system sensed the laser firing for archive purposes.

The flat two–dimensional motor model was designed with a 8.9 mm diameter, glass window port, positioned to allow the laser beam to enter the motor. The glass exit port was a 18.5 diameter window. The windows were placed as close as possible to the propellant to minimize the combustion chamber free volume. A 0-80 screw was mounted outside of the exit window to provide a reference scale in the hologram volume to calibrate the size measurement system. The propellant was mounted between glass plates using RTV using the geometry of Fig. 1. The glass plates would almost always crack during the test, but high–speed motion pictures showed, however, that the cracking usually occurred at the end of the test during the cooling of the plates. This cracking was minimized by the use of borosilicate glass. The cracking did not affect the hologram quality. Of more concern was the possibility of melting glass and of thermal distortion of the glass during the burn. Post–burn analysis of the borosilicate glass plates revealed extensive areas of melted or distorted glass. Despite these problems, the use of borosilicate glass enabled holograms of excellent quality to be obtained. The best results were obtained with thin ($\approx$ 1.0 mm) slabs of propellant operated at relatively low pressures (about 27 atm). Holograms could be successfully obtained for higher pressures (up to 34 atm) and/or thicker propellant slabs (up to 2 mm thick) if the laser was fired sooner after the steady–state burning was achieved. The smaller aluminum powders used gave poorer quality holograms due to the higher density of particle (assuming the same mass loading) and the more uniformly distributed smoke which resulted.

The three–dimensional motor is shown in Fig 2. The motor was cylindrical with a two–inch diameter chamber and a graphite or copper nozzle. The chamber was two inches deep. Optical windows that were 0.75 inches in diameter were placed in the sides. The holograms recorded an approximate 2.5 cm x 2.5 cm x 2.5 cm volume. A annular sample of fuel was placed at one end of the chamber and ignited electronically. The propellant used for most tests consisted of 83.75% AP, 14% HTPB, 2% Al (40 μm diameter) and 0.25% Fe_2O_3.

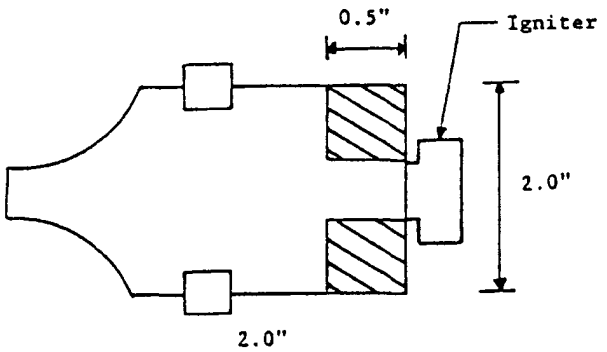

Figure 2: Diagram of experimental three–dimensional motor.

3. HOLOGRAM RECORDING

The laser used to record the holograms was a pulsed Q–switched ruby laser, built by TRW under an Air Force contract, operating at 694.3 nm with an output beam diameter (after an integral beam collimator) of approximately 3.2 cm. The laser pulse energy was one joule with a pulse duration of 50 ns. The pulsed ruby laser used a glass diffuser in its illumination path; this diffuser was necessary to cut down the presence of Schlieren interference fringes produced by the thermal and density gradients surrounding the burning particles in the rocket motor[5].

A holocamera[6], designed by TRW under Air Force contract (along with the pulsed laser), was used both in the hologram recording and reconstruction processes. It consisted of a magnetic mounting plate for the hologram plates and two assisting lenses (to improve hologram resolution and increase the recording dynamic range). The holograms were recorded with a diffuse illumination to avoid the schlieren effects produced by the temperature gradients. AGFA–GEVAERT 8E75 HD holographic plates recorded the hologram. The hologram plates were developed in a darkroom following usual procedures.

4. HOLOGRAM RECONSTRUCTION

The developed hologram was remounted into the holocamera and illuminated with a collimated laser beam, as shown in The reconstruction laser was a 1–watt krypton–ion laser, operating at 647.1 nm. The laser beam illuminated the hologram at an angle of approximately 60°. The real image was focused on a diffusing screen. (To help minimize the effects of the speckle, this screen could be spun, if desired.) The image was viewed with a variable–power microscope. The image could be observed either with the eye or with a low–light–level television vidicon mounted on the microscope. The television images were recorded on a VCR. Optionally, photographs could be recorded with a 35 mm camera.

The diffuse light from the recording interferes with the reference wave of the krypton reconstruction laser. This random interference causes speckle to be introduced into the image. The largest speckle feature was larger than the smallest particle that we wished to resolve in some of the reconstructions, thereby requiring techniques to reduce the speckle. (Techniques to reduce the effect of the speckle are discussed later in this paper.)

5. IMAGE DIGITIZATION AND PROCESSING

Once on video tape, the desired image was played back and digitized by the PC/Vision image processing board controlled by either ImageAction or ITEX/PC software. (The board and software are commercially available from Imaging Technology, Inc.). The digitized image could be filtered immediately or stored for later use.

The steps required to produce the statistical distribution of the particle sizes were:

1. image acquisition from the hologram reconstruction;

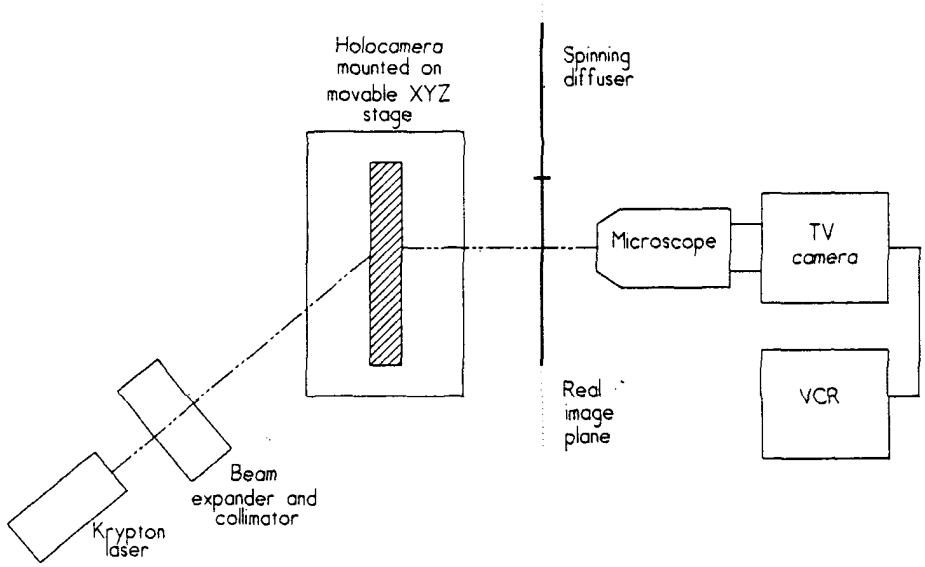

Figure 3: Hologram reconstruction setup.

2. image digitization and storage with the frame–grabber board;
3. speckle reduction filtering to separate the particle image information from the overlaying speckle;
4. application of an image threshold to separate the particle features from the background features;
5. feature identification to find connected feature pixels and to "recognize" the connected pixels as a single object;
6. feature sizing to measure the number of features, the area, x–chord width, and y–chord width; and
7. histogram production using the size data of the prior step.

An IBM PC/AT is the heart of the entire process of image manipulation, from digitizing an image to speckle reduction to the counting of the features. A video image from the VCR can be "grabbed" by the frame–grabber under control of the special software. Each of the picture elements (pixels) in the 512x480 video image array is assigned an integer gray level from 0 to 255 by the frame–grabber. (Level 0 is black; level 255 white.) Each pixel is uniquely addressable and its gray level is alterable, thereby providing the ability to perform digital filtering.

Ideally, the feature data in an image would be very different in gray level from the background, as in Figure 4a. A threshold could then be placed at a level midway between them with the result that the feature particles would be black and the background white. The programs that we developed could then be used to properly size and count the particles of interest. In practice, Figure 4b is much more likely. The particles cover much of the range of gray levels, as does the background speckle. In particular, the ranges of particles and background can overlap. A threshold placed in an unfiltered image would cause portions of some particles to disappear while part of the speckle would appear as particles. What was required was a method to process out the unwanted speckle noise in the background. With a clear separation between the particles of interest and the background, a threshold could then be applied with success.

6. TEST OBJECTS

Three test objects have been used in our investigations to provide a resolution calibration. These objects were imaged under white light as the highest contrast images with the most benign background. The objects were also recorded in holograms in the test setup to duplicate the test geometry.

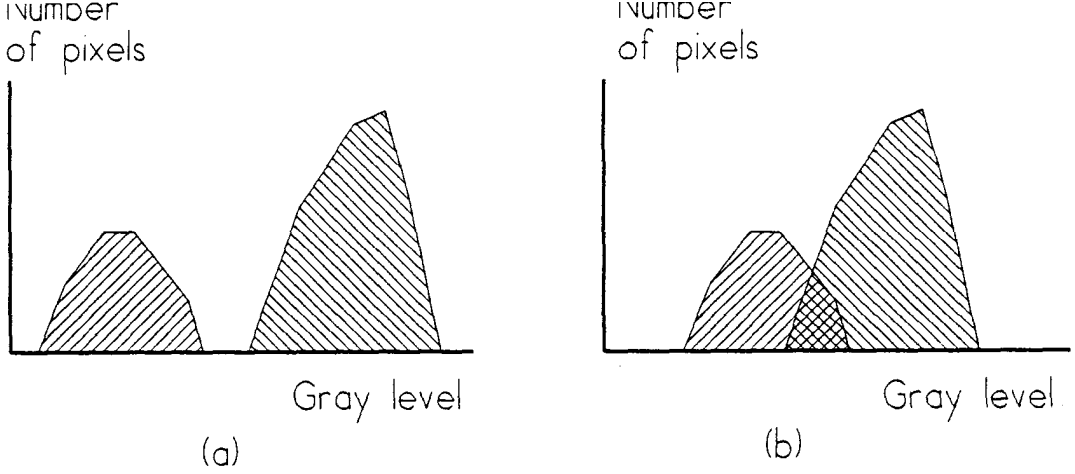

Figure 4: (a) Ideal separation of dark object pixels from bright background pixels and (b) typical overlap of object and background.

- The first object was a calibration reticle produced by LEOS Inc. that consisted of approximately 10,000 photo–deposited opaque circular features of twenty–three diameters ranging from five to ninety–three μm, arranged within an eight–mm diameter circular region. A rectangular array of opaque circles at each of twenty–three diameters was also located on the reticle.
- The second object was the 1951 USAF Standard Resolution chart. This object was used for resolution studies as it provides a more continuous measurement of resolution degradation than the LEOS calibration array.
- The final object was the reconstruction from rocket motor holograms recorded during motor firings.

7. SPECKLE REDUCTION

Edwards[7] explored three speckle reduction algorithms suggested by work in the field of synthetic aperture radars. Improved resolution and speckle reduction was observed with these techniques. Carrier[8] investigated the possibility of digitally averaging images with different speckle patterns to reduce the speckle. He also quantified the speckle reduction due imaging the reconstruction on the spinning mylar disk for comparison with the other speckle–reduction techniques.

Speckle has the characteristics of random multiplicative noise in the sense that the noise level increases with the average gray level of a local area[9]. The presence of speckle reduces one's ability to resolve fine detail. Crimmins[10] showed that the ratio of local deviation to local mean was a reasonable quantitative measure of speckle, due to the multiplicative nature of speckle noise, and defined this ratio as the *speckle index* as a quantitative measure of the amount of speckle in an image. We used this speckle index as our measure of speckle.

7.1. Speckle–reduction filters

Three filters were implemented in software. Two filters depend to a certain degree on the statistics of the image. The third filter uses a geometric hulling algorithm. Detailed mathematical descriptions of the filters are found in the references.

- The sigma filter: The first speckle reduction filter[11] is based on the standard deviation of a Gaussian distribution. By definition, 95.5% of all the pixels fall within two standard deviations on either side of the mean. Any pixels within two standard deviations of a given pixel's gray level are included in an averaging scheme, whereas those outside the "2–sigma" range are excluded. If a particular pixel is considerably different from its neighbors, perhaps none of the neighbors will be within the 2–sigma range. This would indicate a very sharp feature. To avoid the possibility that this sharp feature will not be subject to the averaging process at all, a cutoff is established. If

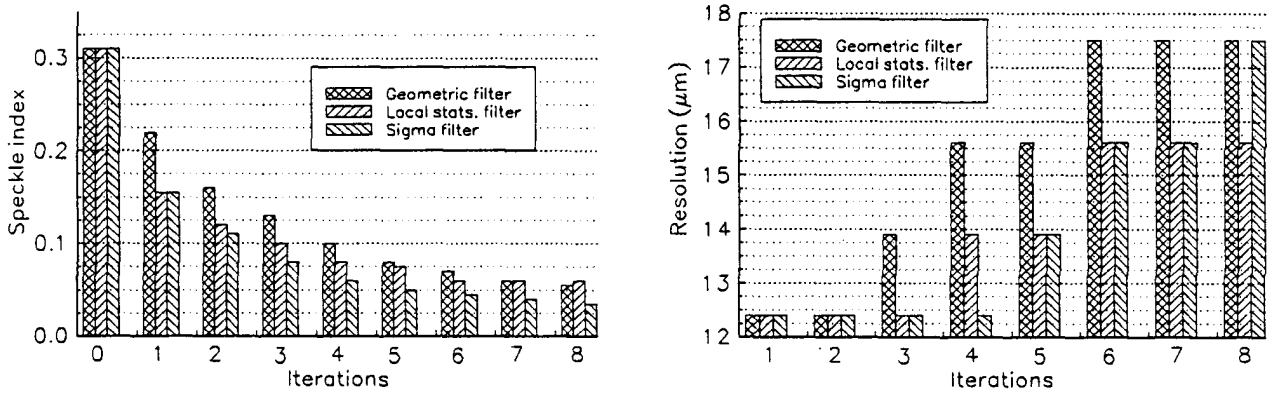

Figure 5: Reduction in speckle index after each iteration for the three speckle–reduction filters and measured image resolution (Air Force resolution target) after each iteration for the three speckle–reduction filters..

the total number of pixels inside the 2–sigma range is less than this minimum cutoff number (2 was chosen), the four–neighbor average then replaces the central pixel's gray level value.

- The local statistics filter: This filter[11] uses local estimates of the mean and variance in a 5x5 window about the central pixel in question. Based on these results, the gray level at the center is left unchanged, is replaced by the average of the pixels in the 5x5 block, or some linear combination of the two.

- The geometric filter: Whereas the previously discussed filters depend to a certain degree upon the statistics of the image to be filtered, the geometric filter[10,12] is based on nonlinear geometric concepts. It is a one–dimensional routine which is run horizontally, vertically and then in the two diagonal directions. In each direction it applies a geometric hulling algorithm to the image and then to the image's complement.

7.2. Comparison of the filter results

The filters were compared in how much speckle they remove per iteration, the computation time per iteration, histogram differences, and visual differences after thresholding the images.

- Speckle reduction: The left side of Figure 5 plots the value of the speckle index after each iteration of the filter. The sigma and local statistics filters both reduced speckle by almost a factor of two after only one iteration, but then dramatically "slowed down" with increased iterations. This may be attributed to the fact that both filters are actually various themes on the blurring technique. More iterations serve to merely increase the blur. Figure 5 shows that the geometric filter's curve was more gradual, allowing the user to stop at a less severe level of filtering. This is a particularly desirable trait, because resolution degradation becomes a problem after only a few iterations.

- Resolution: Reduction of speckle causes a loss of resolution. The right side of Figure 5 shows a comparison of the measured resolution for each of the filter types. The horizontal axis shows the number of iterations of the filter. It is observed that the measured resolution degrades from about 12 μm to almost 18 μm after several iterations of the filters. The geometric and local statistics filters are comparable to each other up through seven iterations, and are superior to the sigma filter in preserving the resolution of the image.

- Computation times: The times for an iteration of each filter are in Table 1. The local statistics filter is slow due to the nested do–loops, frequent calls to subroutines, and a large number of calculations required inside each do–loop.

- Images after thresholding: The ultimate test of any procedure dealing with images is how the thresholded images look after processing. Based on numerous runs of the filters, the geometric filter is judged best at retaining the edges, basic feature shapes, and the size of objects of interest while beating down the speckle. All three filters produced histograms generally similar in shape and distribution.

FILTER	RELATIVE TIME
Sigma	1
Geometric	2.57
Local Statistics	5.42

Table 1: Normalized computation times per iteration (512x512 image)

7.4. Moving–screen averaging

Another speckle–reduction technique is to record the desired image when focused on a moving screen. If the screen moves, then the speckle pattern will change while the particle images will remain constant. If the speckle pattern changes during the integration time of the detector (1/30th of a second for a TV camera), the averaging effect of the detector integration will cause the speckle to average out while the particle images remain the same. We implemented this technique by focusing the real reconstructed images on a spinning translucent diffuse surface and focussing the microscope on this image (as seen in Figure 3). Our measured value of speckle index for this technique is 0.0593 and the measured resolution is 12.4 microns. These values of speckle index and resolution are comparable to the best of the nonlinear speckle–reduction filters after several iterations. In terms of ease of implementation and speed, this moving–screen averaging technique is far superior to the nonlinear filters. *It is recommended that all hologram reconstruction* images be recorded from images focused on a moving screen and that the speckle–reduction filters be used only to further reduce the speckle.

7.5. Multiple–image averaging

We wanted to find out just how good the speckle index value of 0.0593 and the achieved resolution of 12 micrometers were, compared to a simple averaging technique. In the simple averaging technique[13], N separate images with the same resolution–chart image but different speckle patterns were recorded and digitized. Then N digitized images were then successively registered and averaged in the computer with the result displayed on the screen. The speckle index was calculated from the averaged image and the resolution was measured by from the image of the resolution chart. This method is known to theoretically produce a reduction in speckle that is proportional to $1/\sqrt{N}$.

The left side of Figure 6 displays the relative value of speckle index as a function of the number of averaged images N. (Since we are interested in the reduction of speckle index, we have normalized the speckle index to the value for $N = 1$.) The dashed curve shows the theoretical reduction in speckle as $1/\sqrt{N}$. Relatively good agreement is shown. Differences are probably attributable to small registration problems with the images to be averaged. The solid line on the graph shows the speckle index measured from an image taken with the moving screen. The data show that the moving screen technique is better than the averaging of over 25 separate images. Further reduction in the speckle by averaging even more images is not advised, since the knee of the speckle–reduction curve has been passed and the averaging of many more images would be required to achieve only minimal reduction in speckle.

The right side of Figure 6 shows the measured resolution of the averaged images. Contrary to the application of the convolution filters or nonlinear speckle reduction filters, the resolution of the result improves to a value of 16 μm rather than degrades. This improvement is due to the removal of the overlying speckle that masks the smaller features. (The ultimate resolution is determined by the limitations of the hologram recording and reconstruction geometry and the ability of the technique to exactly align the multiple images being averaged.) As the speckle is reduced, the resolution improves by almost a factor of two. (The measured resolution is quantized to the values of the AF Resolution chart.) Also shown in Figure 6, for reference, is the measured resolution of the image recorded with the moving screen. It is seen that the resolution of the image from the moving screen has better resolution than the best of the averaged images.

7.6. Speckle–reduction summary

As a result of our analyses, we concluded that the best method of reducing the speckle is to record the image off of a moving screen. The screen must move fast enough to allow sufficient integration of the image over the 1/30th second frame time of the imaging tube. Modest rotation rates proved capable of providing enough velocity for our disk. While all three nonlinear filters are superior to current linear blurring digital techniques, the geometric filter was found to be the best of the three. It combines the ability to hold the edges and shape of objects with the desirable trait of less

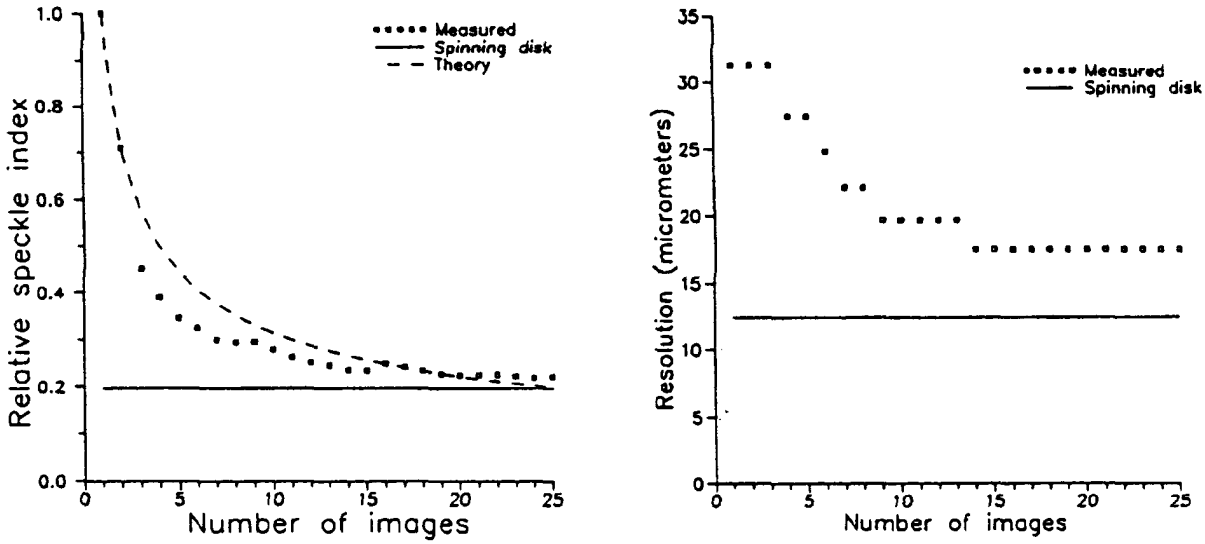

Figure 6: (Left) Measured and theoretical speckle index reduction for averaging images. (Also shown for reference is the speckle index value achieved with a spinning screen). (Right) Measured resolution (USAF resolution target) for averaging images. (Also shown for reference is the resolution achieved with a spinning screen).

filtering per iteration. In this way, the user has more control over the amount of filtering to be done and to what degree the speckle will be reduced. While the geometric filter has been found to be the best overall filter, it may not be superior in every particular circumstance. It has been noted that due to the discrete jumps in speckle index which occur after every iteration, one filter may be able to reach the region of optimum filtering when another cannot. For this reason, the local statistics filter should be used along with the geometric filter and the results after 2 or 3 iterations compared.

Resolution of the original image was about 12 microns. This was degraded to about 14 microns in the filtered images. It is doubtful that much more improvement can be made toward reducing the speckle degradation due to filtering. Any further resolution improvements will most likely have to occur in the recording and reconstruction process, and better optics. Later results[7] measured resolutions typically of 8 microns, and in certain cases, 4 microns. Taking into account the degradation after filtering, a conservative estimate of 10 microns resolution was possible in the finished filtered and thresholded image.

Digital averaging of images is not recommended when the moving–screen averaging technique can be used. Digital averaging requires large amounts of disk storage for the images recorded and a fairly long time to perform the average (due mainly to the disk reading operations required). It does serve as a useful benchmark, however, for comparison of the other imaging techniques as the mathematical description of the frame–averaging technique is well understood.

8. MEASUREMENT RESULTS

Calibration holograms were made to determine the limits of the resolution of the hologram system without the motor firing. Holograms were made using either the pulsed ruby laser or the krypton laser. Both collimated and diffuse illumination were used for comparison, although only the diffuse illumination could be used when the motor fired. The resolution objects were either the LEOS object or the USAF resolution bar chart. Table 2 shows that the expected resolution limit was typically 10 μm with the diffuse illumination and less than 5 μm with collimated light..

The reconstructions of holograms made with the resolution objects were automatically sized to verify the correctness of the processing technique. Reconstructions from holograms made during the test firings were also studied[14]. Figure 7 shows a representative frequency histogram of particle size distribution as measured from an experimental hologram taken during a rocket firing. The horizontal axis is the x–width of the particle. The data represents 1,592 particles that were obtained by combining the data from 16 different regions in the hologram reconstruction. This mosaic approach is necessary since images containing a large number of particles do not have the required resolution to measure the smaller

Illuminator	Object	Type	Resolution
Krypton	USAF	Diffuse	8.8 μm
		Collimated	3.5 μm
	LEOS	Diffuse	11.6 μm
		Collimated	6.8 μm
Ruby	USAF	Diffuse	8.8 μm
		Collimated	8.8 μm
	LEOS	Diffuse	11.6 μm
		Collimated	8.9 μm
Windowed Ruby	USAF	Diffuse	9.9 μm
		Collimated	4.4 μm

Table 2: Resolution results of hologram system calibration.

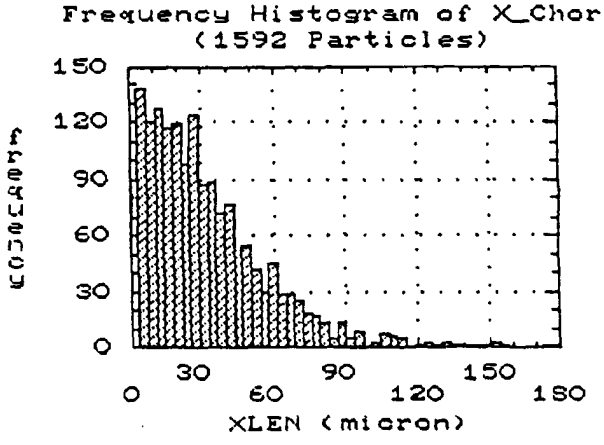

Figure 7: Histogram of particle sizes (in μm) for 1,592 particles contained in 16 fields of view.

particles. Enlarged subimages with the required resolution had too few particles to obtain a statistically meaningful sample.

9. SUMMARY

This work has shown that computer image processing can be used to locate and size particles in a hologram reconstruction.

Algorithms were developed for the Imaging Technology image processing boards made for installation in AT-compatible computers. These boards and their associated software offer a cost-effective way to digitize, store, and process the images. Images of test objects recorded in white illumination and as holograms were successfully processed and served to validate the algorithms. Data from reconstructions of holograms made of a test motor firing were also successfully processed. Comparison with other measurement techniques is required to validate the measured results from the test firings.

Speckle-reduction was required due to the pronounced speckle that overlay our reconstructed images. Removal of the speckle comes at the cost of reduced resolution capability and increased processing time. The speckle index can be used to quantitatively compare the amount of speckle in an image. The resolution was best measured from holograms and images of the Air Force standard resolution chart. The best speckle-reduction technique for our images was to record the images from a moving diffuse screen. The integration of the image by the TV tube reduced the speckle considerably. Of the nonlinear filters used to reduce speckle in synthetic aperture radar images, the geometric filter

proved to be the best combination of speckle reduction, resolution maintenance, and processing time. Techniques for digitally averaging the images were successful but required considerable computer storage and processing time to produce an image that was inferior to the moving–screen images in terms of the amount of speckle present. The nonlinear filters and image–averaging techniques might prove useful, however, in reducing the residual speckle found in the moving–screen images.

10. ACKNOWLEDGEMENTS

The authors are pleased to acknowledge the contributions of many thesis students who recorded the holograms and processed the images. The support of the Air Force Phillips Laboratory is also gratefully acknowledged.

11. REFERENCES

1. R.G. Cramer, R.J. Edington, D.E. Faber, K.J. Graham, B.J. Hansen, P.J. Hickey, L.A. Klooster, P.J. Mellin, J.P. Powers, and D.W. Netzer, *An investigation of experimental techniques for obtaining particulate behavior in metallized solid rocket propellant combustion*, Technical Report AFRPL–TR–84–014, Air Force Rocket Propulsion Laboratory, Edwards AFB, CA 93523, 1984.

2. T.D. Edwards, R.K. Harris, K.G. Horton, M.G. Keith, A. Kertadidjaja, Y.S. Lee, D.N. Redman, J.S. Rosa, J.B. Rubin, S.C. Yoon, J.P. Powers, and D.W. Netzer, "Measurements of Particulates in Solid Propellant Rocket Motors (U)," Air Force Astronautics Laboratory Technical Report AFAL–TR–87–029, Edwards AFB, CA, October, 1987.

3. J.P. Powers, *Automatic particle sizing from rocket motor holograms*, Technical report NPS–EC–91–003, Naval Postgraduate School, Monterey CA 93943.

4. K.D. Ahlers and D.R. Alexander, "Microcomputer based digital image processing system developed to count and size laser–generated small particle images," *Optical Engineering*, Vol. 24, No. 6, pp. 1060–1065, 1985

5. T.D. Edwards, K.G. Horton, D.N. Redman, J.S. Rosa, J.B. Rubin, S.C. Yoon, J.P. Powers, and D.W. Netzer, "Measurements of Particulates in Solid Propellant Rocket Motors," *Proceedings of the 21st JANNAF Combustion Meeting*, Chemical Propulsion Information Agency, Johns Hopkins University, Laurel, Maryland, pp. 1–14, 1987.

6. R.F. Wuerker and R.A. Briones, *Instruction manual for the improved ruby laser holographic illuminator*, Technical Report AFRPL–TM–78–12, Air Force Rocket Propulsion Laboratory, Edwards AFB, CA 93523, 1978.

7. CPT T.D. Edwards, *Implementation of three speckle reduction filters for solid propellant combustion holograms*, MSEE Thesis, Naval Postgraduate School, Monterey, CA, December 1986

8. MAJ D.J.G. Carrier, *Automatic measurement of particles from holograms taken in the combustion chamber of a rocket motor*, MSEE Thesis, Naval Postgraduate School, Monterey, CA, December 1988

9. J.W. Goodman, "A random walk through the field of speckle," *Optical Engineering*, Vol. 25, No. 5, pp. 610–612, 1986.

10. T.R. Crimmins, "Geometric Filter for Speckle Reduction," *Applied Optics*, Vol. 24, No. 10, May 1985.

11. J.S. Lee, "Speckle Suppression and Analysis for Synthetic Aperture Radar," *Optical Engineering*, Vol. 25, No. 5, May 1986.

12. T.R. Crimmins, "Geometric Filter for Reducing Speckle," *Optical Engineering*, Vol. 25, No. 5, May 1986.

13. J.S. Lim and H. Nawab, "Techniques for speckle noise removal," *Optical Engineering*, Vol. 20, No. 3, pp. 472–480, 1981

14. LT(jg) E.S. Orguc, *Automatic data retrieval from rocket motor holograms*, MSEE Thesis, Naval Postgraduate School, Monterey, CA, December 1987